CASSCF Study of Bonding in NiCO and FeCO

XIN XU,[1] XIN LÜ,[1] NANQIN WANG,[1] QIANER ZHANG,[1] MASAHIRO EHARA,[2] HIROSHI NAKATSUJI[2]

[1] *State Key Laboratory for Physical Chemistry of Solid Surfaces, Institute for Physical Chemistry, Department of Chemistry, Xiamen University, Xiamen 361005, People's Republic of China*
[2] *Department of Synthetic Chemistry and Biological Chemistry, Faculty of Engineering, Kyoto University, Kyoto 606, Japan*

Received 19 May 1998; revised 3 October 1998; accepted 20 October 1998

ABSTRACT: A series of CASSCF calculations were performed on the ground states of NiCO and FeCO. The contributions of the σ/π interactions are checked by examining the validity of the CASSC calculation to describe the molecule with a particular choice of the active space. The calculation results substantiate that the stability of MCO is determined by a balance between π donation from the metal $3d_\pi$ to the CO 2π and repulsion between the metal σ electrons and the CO 5σ lone pair and, at the same time, emphasizes the importance of the synergistic σ/π interactions between the metal and the CO group. The relative importance of σ/π interactions depends on the nature of the metal. In the case of NiCO, it is the π donation from Ni $3d_\pi$ to CO 2π that makes the largest contribution to the formation of the Ni—CO bond, while in the case of FeCO, it is the correlation of σ electrons that holds the metal and CO together. Int J Quant Chem 72: 221–231, 1999

Introduction

There is a great deal of interest in understanding the bonding in transition-metal monocarbonyls (see, e.g., [1–3] and references therein). The importance of this kind of study is twofold: First, it provides a system which can be taken as an archetype in studies of the coordinate bonds without any interference arising from, for example, the conjugation effects between ligands, and second, it offers a zeroth-order model for interpreting the chemisorption of the CO molecule on a metal surface, with the understanding of catalytic activation processes as a target.

Owing to the pioneer work of Blyholder [4], the M—CO bond is interpreted as arising from a synergistic combination of σ donation from the filled

Correspondence to: X. Xu.

Contract grant sponsors: National Natural Science Foundation of China; State Education Commission of China; Fok Ying Tung Education Foundation; Japan Society for Promotion of Science.

CCC 0020-7608 / 99 / 030221-11

CO 5σ orbital to the metal and π backdonation from the metal d_π to CO 2π. Population analyses show an electron density decrease in the CO σ space, in conjunction with an electron density increase in the CO π space, giving a bonding mechanism which is consistent with this view. Unfortunately, all the population analyses suffer from the problem of dividing the overlap populations arbitrarily. This problem is serious when large basis sets are employed in the calculations [5, 6]. Bagus et al. proposed an approach named the CSOV (constrained space orbital variation) method [7], which decomposes the interaction into contributions from intraunit, within the metal or the CO units, and interunit, between the metal and CO units, charge redistributions. By means of CSOV, Bauschlicher et al. presented a qualitatively different bonding picture [6, 8], in which the role of the synergistic σ donation and π backdonation was downplayed. They concluded that the π donation, in energetics, is the most important factor for, for example, Fe, Cu, and Ni bonding with CO; the metal–CO σ interaction makes only a minor bonding contribution or is even repulsive [6, 8]. More recently, Blyholder and Lawless, taking the diatomic energy contribution of particular orbitals in a particular bond to the stability of the total molecular energy as a new criterion [9], reclaimed the importance of the σ donation. Following their MNDO calculations, they argued that the largest contribution to the metal–carbonyl bond is provided by the σ electrons. Thus, the role of σ bonding has become controversial. People are wondering what the relationship between the Blyholder model and the Bagus model is [10].

Another point of controversy concerns the degree of mixture between the Ni $3d^{10}$ and $3d^9 4s^1$ configurations in the description of the bonding for the ground state $^1\Sigma^+$ of NiCO. The NiCO $^1\Sigma^+$ was at first thought to be a Ni $^1S(3d^{10})$-derived closed-shell state [11], since NiCO would be regarded as a small piece of $Ni(CO)_4(^1A_1)$ in the same metal configuration. Although the Ni $3d^{10}$ is ideal for bonding [12], it requires 1.74 eV for the excitation from Ni $^3D(3d^9 4s^1)$ to $^1S(3d^{10})$ [13]. Examination of the CI wave function of NiCO $^1\Sigma^+$ leads to a description of the ground state as a mixture of 60% Ni $3d^{10}$ and 40% Ni $3d^9 4s^1$ [14]. On the other hand, Blomberg et al. argued that nickel is best described by a $3d^9 4s^1$ configuration, since nickel in NiCO $^1\Sigma^+$ has a d population very close to nine [15]. The repulsion between CO 5σ and Ni $4s$ is effectively reduced by sd_σ hybridization without paying for the high cost of $4s \rightarrow 3d$ electron excitation. Another way of reducing σ repulsion is the sp_σ hybridization, especially when the $d\sigma$ and $4s$ orbitals are high-spin-coupled so that sd_σ hybridization is not feasible.

We performed a series of complete active space SCF (CASSCF) [16, 17] calculations on the ground states NiCO and FeCO in the hope that a comparison of the results with a different choice of active orbitals will shed light on the relative importance of various electron correlation effects, help to clarify the relative importance of the σ/π interaction, and thus gain insight into the nature of metal–carbonyl bonding.

Computational Details

Our theoretical journey begins with a Hartree–Fock (HF) calculation. Since the ground state of NiCO is generally accepted as $^1\Sigma^+$ [11, 14, 15], the restricted HF (RHF) wave functions of $^1\Sigma^+$ NiCO have been taken as the initial guess for the following CASSCF calculations. At the first step of route 1, only the metal $3d_\sigma$ and $4s$ orbitals were correlated [denoted as $(3d_\sigma, 4s)^2$]. This is a CAS of two electrons in two active orbitals [CAS(2, 2), in short], which allows one to take the Ni sd_σ hybridization into account. Second, the CO 5σ MO was added, giving a $(3d_\sigma, 4s, 5\sigma)^4$/CAS(4, 3). This CAS(4, 3) calculation correlates the bonding electrons in σ space. The last step of route 1 is to include the filled metal $3d_\pi$ orbitals and the empty CO 2π orbitals in the active space. This results in a $(3d_\pi, 2\pi)^4(3d_\sigma, 4s, 5\sigma)^4$/CAS(8, 7) calculation, which introduces bonding correlation in π space and normally enhances the π donation with respect to HF calculation. Metal $3d_\delta$ electrons are believed to be nonbonding and thus not included in the active space in all CASSCF calculations of Ni—CO. Route 2 is denoted as $(3d_\pi, 2\pi)^4$/CAS(4, 4) $\rightarrow$ $(3d_\pi, 2\pi)^4(3d_\sigma, 4s)^2$/CAS(6, 6) $\rightarrow$ $(3d_\pi, 2\pi)^4(3d_\sigma, 4s, 5\sigma)^4$/CAS(8, 7), which starts from a π bonding correlation and takes a σ bonding correlation into consideration subsequently.

Similar calculations were performed on $^3\Sigma^-$ FeCO, which has been assigned as the ground state of FeCO both experimentally [18] and theoretically [19, 20]. The restricted open-shell HF (ROHF) wave functions of $^3\Sigma^-$ FeCO were employed as the starting point for the subsequent CASSCF calculations. In all CASSCF calculations,

the open-shell $3d_\delta$ electrons are always included in the active spaces. Similarly, Route 1 starts from a σ bonding correlation, while Route 2 begins with π bonding correlation. Both routes end at a 10 electrons in nine active orbitals CAS(10, 9) calculation, which includes all metal valence $3d$ and $4s$ electrons as well as HOMO (5σ) and LUMOs (2π) of CO in the active space.

At all steps of route 1 or 2, we performed geometry optimizations and calculated the vibrational frequencies. All these calculated molecular parameters are compared and contrasted with the experimental values or more accurate theoretical values. The neglect of certain important bonding correlation will lead to deficiencies in the description of electronic structure and the bonding mechanisms in M—CO. By examining the validity of a CASSCF calculation with a particular choice of the active space, the importance of the σ/π interactions and the possible existence of synergistic σ/π interactions can be checked. Taking the total energy of a state, which is essentially nonbounded at the level of Hartree–Fock, as a reference, the degree of total energy lowering in a CASSCF calculation signifies the importance of introducing certain bonding correlation effect, indicating its contribution to the bonding stabilization of M—CO.

Although it is understood that a quantitative description of M—CO bonding demands of correlating all metal valence ($3d$ and $4s$) and ligand valence (3–5σ and 1π) electrons [21, 22], it is well established that the final CAS presented here has contained the essence of M—CO bonding [8, 15, 23]. Furthermore, we should point out that CAS with limited active space would give a biased description of the bonding mechanism, such that interpretation of the calculation results should be made with caution and reservation.

The metal basis sets used in this study were derived from the Wachters ($14s9p5d$) primitive sets [24], which are contracted to [$8s4p3d$] by using the Wachters contraction scheme 3. To these basis sets, two additional diffuse p functions were added, which were optimized by Wachters to describe the $4p$ orbitals and which are scaled by a factor of 1.5 to make them more suitable for molecular calculations [24]. As suggested by Hay [25], a diffuse $3d$ function was also added to give a balanced description of the transition-metal atom involving different d occupation. This leads to a final metal basis set of the form ($14s11p6d$)/[$8s6p4d$]. The C and O basis sets are derived from the van Diujneveldt ($9s5p$) primitive sets [26], which are contracted to [$4s3p$] based on a (5211) contraction of the s space and a (311) contraction of the p space. These basis sets are at least of double-ζ quality and are frequently employed in the theoretical literature [22, 27].

All calculations were performed using Gaussian 94 [28]. The molecular properties of M—CO are calculated with $6d$ (Cartesian d functions), while the Mulliken populations are analyzed with $5d$ (pure d functions) at the optimized geometry of M—CO with $6d$.

Results and Discussion

NiCO $^1\Sigma^+$

The calculated molecular properties of NiCO $^1\Sigma^+$ are presented in Table I. The results of the Mulliken population analysis are given in Table II, where Ni—C is the overlap population, $\Delta\sigma$ is defined as six minus the population of valence orbitals with σ symmetry on the CO fragment, and $\Delta\pi$, as four minus the population of orbitals with π symmetry on the CO fragment. Therefore, $\Delta\sigma$ and $\Delta\pi$ provide the simplest, although unreliable sometimes, way of quantifying the extent of σ donation and π backdonation.

RHF calculation of NiCO $^1\Sigma^+$ gives a picture of strong Ni—CO interaction, for example, significant Ni—C stretching frequency and a large downshift of the C—O stretching frequency with respect to the free CO. This closed-shell NiCO possesses a metal electronic configuration of $3d^{9.481}4s^{0.377}4p^{0.043}$, which lies in between the atomic states of $3d^{10}$ and $3d^9 4s^1$. The bonding energy of RHF NiCO is found to be 1.440 eV with respect to its dissociated limit CO($^1\Sigma^+$) + Ni (d^{10}, ^1S). The strong Ni—CO interaction could be understood in terms of σ donation and π backdonation ($\Delta\sigma = 0.15$; $\Delta\pi = -0.25$), with π backdonation outweighing σ donation.

UHF calculation, however, locates an equilibrium geometry of NiCO with a much longer Ni—C bond distance (5.496 Å in UHF versus 1.739 Å in RHF). This open-shell NiCO has a metal electronic configuration of $3d^9 4s^1$ with a zero overlap population between Ni and CO. The bonding energy of UHF NiCO is only 0.001 eV with respect to its dissociated limit CO($^1\Sigma^+$) + Ni (d^9s^1, ^1D). Although the C—O bond length in UHF NiCO is hardly changed with respect to the free CO, the

TABLE I
Calculated molecular parameters of $^1\Sigma^+$ Ni—CO.

Method	E[a] (eV)	R_e(Ni—C) (Å)	R_e[b](C—O) (Å)	ω_e(Ni—C) (cm^{-1})	ω_e(bend) (cm^{-1})	ω_e[c](C—O) (cm^{-1})
RHF	+2.711	1.739	1.139	490	265	2098
UHF	0.000	5.496	1.124	4.4	14.3	2272
σ Correlation						
CAS(2, 2)	−0.008	5.498	1.124	5.5	16.6	2272
CAS(4, 3)	−0.009	5.498	1.124	5.6	16.5	2272
π Correlation						
CAS(4, 4)	−0.425	1.717	1.176	548	315	1994
σ/π correlation						
CAS(6, 6)	−2.061	1.689	1.159	611	358	2008
CAS(8, 7)	−2.219	1.683	1.161	617	360	2011
CCSD(T)[d]	—	1.687	1.166	592	369	2016[e]

[a] UHF energy (−1619.37670 au) is taken as the reference. Minus indicates energy lowering.
[b] R_e calculated for free CO is 1.124 Å. The experimental value is 1.128 Å [29].
[c] ω_e calculated for free CO is 2435 cm^{-1}. The experimental value is 2170 cm^{-1}.
[d] See [30].
[e] Experimental value after corrections for matrix effects (5 cm^{-1}) and anharmonicity (27 cm^{-1}) is 2028 cm^{-1} [31].

C—O stretching vibrational frequency is strongly perturbed by the presence of Ni (see Table I). As compared and contrasted with RHF NiCO, we may reach such a conclusion that the CO 5σ should be antibonding to the Ni $4s$ orbital. Emptying the Ni $4s$ orbital would minimize the metal–ligand repulsion in the σ space, and, hence, enhance the Ni—CO interaction. Experimentally, the Ni $(d^9s^1, {}^1D)$ atomic state is 1.403 eV lower than Ni $(d^{10}, {}^1S)$ [13], while at our HF level, the energy separation between Ni $(d^9s^1, {}^1D)$ and $(d^{10}, {}^1S)$ is greatly overestimated with $\Delta|(d^9s^1, {}^1D) - (d^{10}, {}^1S)| = 4.15$ eV. Indeed, the bonding contribution in RHF NiCO cannot compensate for the excitation energy from Ni $(d^9s^1, {}^1D)$ to Ni $(d^{10}, {}^1S)$, such that the UHF energy is much (2.711 eV) lower than the RHF energy, even though RHF NiCO is more strongly bonding.

Although HF calculations have given valuable qualitative insight into this and related systems [6–8], more reliable results can only been obtained when the suitable correlation effects have been taken into account. Blomberg et al. showed the importance of sd_σ hybridization which provides an efficient way of reducing repulsion in σ space without paying for the cost of the excitation to the

TABLE II
Mulliken populations for $^1\Sigma^+$ Ni — CO at equilibrium geometries of various levels of approximation.

Method	$3d_\delta$	$3d_\pi$	$3d_\sigma$	$4s$	$4p_\sigma$	$4p_\pi$	$\Delta\sigma$	$\Delta\pi$	Ni—C
RHF	4.00	3.75	1.73	0.38	0.04	0.01	0.15	−0.25	0.19
UHF	4.00	4.00	1.00	1.00	0.00	0.00	0.00	0.00	0.00
σ Correlation									
CAS(2, 2)	4.00	4.00	1.00	1.00	0.00	0.00	0.00	0.00	0.00
CAS(4, 3)	4.00	4.00	1.00	1.00	0.00	0.00	0.00	0.00	0.00
π Correlation									
CAS(4, 4)	4.00	3.26	1.92	0.29	0.08	0.05	0.30	−0.69	0.35
σ/π Correlation									
CAS(6, 6)	4.00	3.44	1.69	0.54	0.07	0.03	0.29	−0.53	0.37
CAS(8, 7)	4.00	3.42	1.68	0.55	0.07	0.04	0.29	−0.54	0.38

$3d^{10}$ configuration [15, 23]. This kind of nondynamical correlation effects would be best described with a multi-configurational, CASSCF-type, reference wave function.

The simplest CASSCF calculation is CAS(2, 2), with two σ electrons in the $3d_\sigma$ and/or $4s$ orbital. Taking the wave functions of RHF NiCO $^1\Sigma^+$ as an initial guess, the CAS(2, 2) calculation gives a result which is very closed to UHF NiCO $^1\Sigma^+$. Further inclusion of the CO 5σ into the active space has a negligible effect on the calculated properties with respect to those of CAS(2, 2). Thus, σ donation would have made a minor contribution to Ni—CO bonding and the fact that the interaction in the σ space is mainly repulsive is further revealed, agreeing well with that reached by Bagus et al. with the CSOV method [6–8]. It is also obvious that only considering the bonding correlation in σ space does not provide reasonable description of the Ni—CO bonding.

Let us now start from the first step of route 2: CAS(4, 4) calculation. Inclusion of the Ni-filled $3d_\pi$ orbitals and the CO empty 2π into the active space enhances the π backdonation from Ni $3d_\pi$ to CO 2π with respect to RHF NiCO, which leads to a longer C—O distance [1.176 Å in CAS(4, 4) versus 1.139 Å in RHF] and a shorter Ni—C distance [1.717 Å in CAS(4, 4) versus 1.739 Å in RHF]. These observations would also be rationalized with the calculated vibrational shifts, that is, an increase of the Ni—C stretching frequency and a decrease of the C—O stretching frequency. The CAS(4, 4) calculation leads to a NiCO with substantially low total energy, resulting in the $^1\Sigma^+$ state being the ground state. Therefore, the bonding correlation in π space is very important for a reasonable description of the Ni—CO interaction. This result may also suggest that the π donation is, in energetics, the most important factor for Ni bonding with CO, in good agreement with the CSOV results of Bagus et al. [6–8].

If the electron in the Ni $4s$ is mainly repulsive to the electrons in the CO 5σ, one may expect that further inclusion of Ni $3d_\sigma$ and $4s$ orbitals into the $(3d_\pi, 2\pi)$ active space would lengthen the Ni—C distance and destabilize the NiCO bonding because of the increase of the $4s$ population. The fact is almost the contrary. The CAS(6, 6) calculation indeed brings about an increase of $4s$ occupation; the Ni—C distance is, on the other hand, becoming shorter and the Ni—C stretching frequency larger, indicating a further stabilization of the NiCO bonding.

To give a further comparison between the wave functions of CAS(4, 4) without σ correlation and those of CAS(6, 6) with σ correlation, we depicted the orbital contour plots, as well as the difference contour plots. Figure 1 presents MO plots in the σ space [the MO plots in the π space of CA(4, 4) and CAS(6, 6) are similar and therefore not shown]. The difference contour plots, shown in Figure 2, are obtained by the electron density from CAS(6, 6) minus that from CAS(4, 4). The differences of the contour plots with and without $(3d_\sigma, 4s)$ correlation are illuminating. The sd_σ hybridization provides an efficient way to reduce the σ repulsion

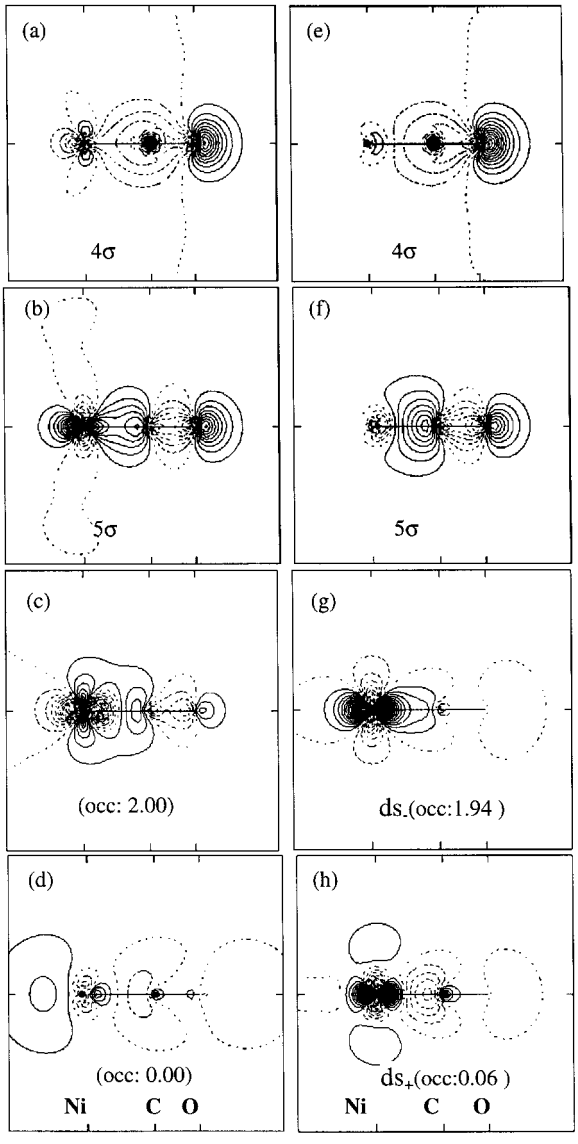

FIGURE 1. σ MO plots of $^1\Sigma^+$ NiCO: (a)–(d) from CAS(4, 4); (e)–(h) from CAS(6, 6).

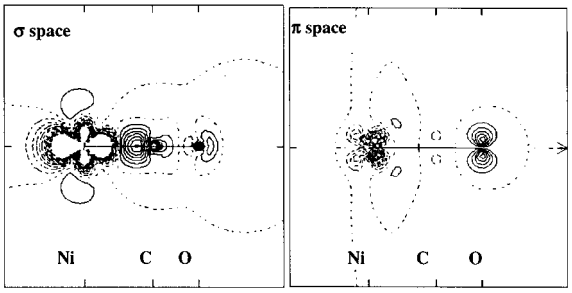

FIGURE 2. $^1\Sigma^+$ NiCO difference contour plots between $(3d_\pi, 2\pi)^4(3d_\sigma, 4s)^2$/CAS(6, 6) and $(3d_\pi, 2\pi)^4$/CAS(4, 4). Dashed lines indicate electron loss while solid lines indicate electron gain.

between Ni and CO 5σ [cf. (c) and (g) in Fig. 1]. On the other hand, the increase of the $4s$ population change Ni—CO from σ bonding to antibonding [cf. (b) and (f) in Fig. 1]. The overall effect is that the introduction of $(3d_\sigma, 4s)$ correlation decreases the σ donation from CO 5σ to Ni, while the relieving of σ repulsion by means of sd_σ hybridization enhances the π donation from Ni $3d_\pi$ to CO 2π, as shown in Figure 2. Therefore, the further stabilization of the NiCO bonding after introduction of $(3d_\sigma, 4s)$ correlation would be best described as an increase of π donation and a decrease of σ repulsion.

The Ni—C and C—O distances calculated with CAS(6, 6) are 1.689 and 1.159 Å, respectively, which are in satisfactory agreement with the results of larger CAS(8, 7) and with the most accurate results update. Those are Ni—C 1.687 Å [30], 1.677 Å [32], and C—O 1.166 Å [30] obtained with high-quality single, double, and perturbative triple excitations coupled cluster [CCSD(T)] calculations. The CAS(6, 6), including both π bonding and sd_σ hybridization, constitutes the smallest active space possible to give a qualitatively correct picture of the NiCO bonding. Neither CAS(2, 2) with only sd_σ correlation or CAS(4, 4) with only π correlation is good enough to lead to a suitable description of Ni—CO bonding. This fact itself signifies the importance of the interdependence of σ/π interactions.

The importance of concerted σ/π contributions to the stability of NiCO is further revealed after the inspection of the correlation energy introduced at each step of route 1 or 2 (see Table I). Taking the energy of UHF NiCO, which is essentially nonbounded, as a reference, the first two steps of route 1, which correlate only the σ electrons, brings about a limited correlation energy (-0.01 eV). On the other hand, the first step of route 2, which correlates only the π electrons, brings about a large correlation energy (-0.43 eV). This suggests taht π electrons make a larger contribution to the Ni—CO bonding than to the σ electrons. The second step of route 2, which includes both π bonding and sd_σ hybridization in the active space, leads to substantially large bonding stabilization. The correlation energy introduced at this step (-2.06 eV) greatly exceeds the summation of the separate contributions from σ and π electrons ($-0.01 - 0.43 = -0.44$ eV), providing clear evidence of the synergistic contributions of σ/π electrons. Further inclusion of 5σ into the active space leads to further stability of NiCO ($-2.219 + 2.061 = -0.157$ eV).

Nickel–carbonyls have conventionally been considered as having a $3d^{10}$ configuration on nickel [15, 23]. The main reasons are that the ground states of the nickel–carbonyls can be described by one closed-shell configuration and the Ni $4s$—CO 5σ σ repulsion is minimized in a d^{10} configuration. Blomberg et al. were the first who argued that nickel is close to $3d^94s^1$ rather than to $3d^1$ in NiCO, since they obtained a $3d$ population very close to 9(9.16) [15, 23]. Blomberg et al. further pointed out that sd_σ hybridization efficiently reduces the σ repulsion and a $3d^94s^1$ occupation on nickel can very well be described by one close-shell configuration in these hybridized orbitals [15, 23]. The basis sets and methods employed here are almost the same as those of Blomberg et al. [15, 23]. Thus, we have obtained very similar results. MO plots [(g) and (h) in Fig. 2] clearly show the ds_- hybrid with electron density perpendicular to the C—O axis is almost doubly occupied (1.94), while the ds_+ hybrid with electron density along the C—O axis is almost empty (0.06). The CI weight of the main configuration-state function in the CAS wave function is 0.88.

Taking Ni $^1D(3d^94s^1)$ or Ni $^1S(2d^{10})$ as the reference state would lead to a different interpretation of bonding mechanism in NiCO. If NiCO is considered as a $3d^{10}$-derived state, changes of the Ni orbital populations indicate that the Ni $4s$ orbital accepts some electrons from CO 5σ, and to reduce the repulsion between two-orbital $(3d_\sigma, 5\sigma)$ four-electron interaction, some $3d_\sigma$ electrons should be transferred to Ni $4sp_\sigma$ orbitals. On the other hand, if NiCO is considered as a $3d^94s^1$-derived state, population changes show that the Ni $3d_\sigma$ is the orbital to accept electrons, and to reduce the repulsion between $4s$ and 5σ orbitals, some $4s$

electrons should be excited into the Ni $3d_\sigma$ orbital. Clearly, taking $3d^9 4s^1$ as the reference state results in a bonding mechanism which is in accordance with the screening mechanism, that is, the increase of the occupation in the $3d_\sigma$ orbital due to σ donation from CO 5σ and excitation from Ni $4s$ is to compensate for the decrease of the occupation in the $3d_\pi$ orbitals back to the π backdonation to CO, so as to minimize the charge buildup. Since sd_σ hybridization here only changes the shape of $3d$ or $4s$ orbitals and does not affect the occupation in the relative orbitals, the promotion of $4s$ electrons to $3d_\sigma$ can only be understood by means of $3d^9 4s^1/3d^{10}$ mixing. Therefore, although the Ni $^1D(3d^9 4s^1)$ configuration occurs at the dissociation limit of the NiCO $^1\Sigma^+$ state, the Ni d^{10} configuration is important near the equilibrium geometry of this state.

FECO $^3\Sigma^-$

In Tables III and IV, we present the calculated molecular parameters as well as the results of Mulliken population analysis for FeCO $^3\Sigma^-$. The bonding mechanisms in FeCO $^3\Sigma^-$ will be compared and contrasted with those in NiCO $^1\Sigma^+$.

ROHF calculation of FeCO $^3\Sigma^-$ results in a state which is essentially nonbounded [R_e(Fe—C) = 6.166 Å; R_e(C—O) = 1.124 Å]. The bonding energy of ROHF FeCO $^3\Sigma^-$ is only 0.001 eV with respect to its dissociated limit calculated at free CO bond length (1.124 Å) and R(Fe—C) = 50.0 Å. The electronic configuration of Fe is found to be $3d^6 4s^2$ with two high-spin coupled $3d_\delta$ electrons and four $3d_\pi$ electrons (see Table IV). In the UHF calculation, one $4s$ electron is excited into the $3d_\sigma$ orbital, giving an Fe of $3d^7 4s^1$. This greatly reduces the Fe $4s$—CO 5σ σ repulsion and leads to a bounded state [R_e(Fe—C) = 1.1914 Å; R_e(C—O) = 1.145 Å] with a bonding energy of 0.228 eV. At the dissociated limits, the energy gap between ROHF and UHF FeCO $^3\Sigma^-$ is 0.861 eV, which corresponds well to the experimental energy separation, 0.812 eV, between $d^6 s^2(^3P)$ and $d^7 s^1(^3F)$.

Taking ROHF wave functions as the starting point, we performed a series CAS calculations of various active spaces. The open-shell spin-paralleled $3d_\sigma$ orbitals are always included in the active space. The smallest active space which correlates $3d_\sigma$ and $4s$ electrons is $(3d_\sigma, 4s)^2(3d_\delta)^2$. This CAS(4, 4) calculation leads to a state which is more or less bounded [R_e(Fe—C) = 2.050 Å; R_e(C—O) = 1.125 Å]. Although the bond distance between C and O is only slightly perturbed, correlation between $3d_\sigma$ and $4s$ has succeeded in promoting one $4s$ electron to the $3d_\sigma$ orbital and holding Fe and CO fragments together. Further inclusion of the CO 5σ orbital into the active space has only a

TABLE III
Calculated molecular parameters of $^3\Sigma^-$ Fe—CO.

	E[a] (eV)	R_e(Fe—C) (Å)	R_e[b](C—O) (Å)	ω_e(Fe—C) (cm^{-1})	ω_e(bend) (cm^{-1})	ω_e[c](C—O) (cm^{-1})
ROHF	0.000	5.166	1.124	14.2	18.9	2272
UHF	−1.088	1.914	1.145	371	272	1941
σ Correlation						
CAS(4, 4)	−0.628	2.050	1.125	245	278	2213
CAS(6, 5)	−0.634	2.047	1.125	248	279	2211
π Correlation						
CAS(6, 6)	−1.159	5.166	1.124	12.4	19.5	2272
σ/π Correlation						
CAS(8, 8)	−3.225	1.775	1.161	422	351	1933
CAS(10, 9)	−3.447	1.774	1.167	465	344	1953
Expt.[c]	—	1.719[d]	1.209[d]	530	330	1950

[a] ROHF energy (−1374.93854 au) is taken as the reference.
[b] R_e calculated for free CO is 1.124 Å. The experimental value is 1.128 Å [29].
[c] ω_e calculated for free CO is 2435 cm^{-1}. The experimental value is 2170 cm^{-1}.
[d] Results of MCPF calculation [22].
[e] See [18].

TABLE IV
Mulliken populations for $^3\Sigma^-$ Fe—CO at equilibrium geometries of various levels of approximation.

Method	$3d_\delta$	$3d_\pi$	$3d_\sigma$	$4s$	$4p_\sigma$	$4p_\pi$	$\Delta\sigma$	$\Delta\pi$	Fe—C
ROHF	2.00	4.00	0.00	2.00	0.00	0.00	0.00	0.00	0.00
UHF	2.00	3.55	1.03	0.86	0.32	0.08	0.21	−0.37	0.28
σ Correlation									
CAS(4, 4)	4.00	4.00	1.00	1.00	0.19	0.01	0.11	−0.11	0.11
CAS(6, 5)	4.00	4.00	1.00	1.00	0.19	0.01	0.11	−0.11	0.11
π Correlation									
CAS(6, 6)	2.13	3.87	0.00	2.00	0.00	0.00	0.00	0.00	0.00
σ/π Correlation									
CAS(8, 8)	2.01	3.38	1.26	0.95	0.11	0.06	0.33	−0.55	0.37
CAS(10, 9)	2.01	3.36	1.26	0.94	0.12	0.06	0.32	−0.57	0.38

small effect on the description of Fe—CO bonding. Further introduction of the correlation effects in π space, however, greatly improves the quality of calculation. The calculation results with $(3d_\pi, 2\pi)^4(3d_\sigma, 4s, 5\sigma)^4(3d_\delta)^2$/CAS(10, 9) are in good agreement with the modified coupled-pair functional (MCPF) calculation which correlated all 18 valence electrons of FeCO [22] (see data in Table III).

To distinguish the relative importance of σ correlation versus π correlation, we may start our theoretical journey by considering π correlation first. Taking ROHF wave functions as the starting point, we performed the $(3d_\pi, 2\pi)^4(3d_\delta)^2$/CAS(6, 6) calculation. The optimization locates a long Fe—C distance (5.17 Å). This clearly shows that the strong σ repulsion between the doubly occupied $4s$ and 5σ keeps Fe and CO apart and the π donation from $3d_\pi$ to 2π cannot be operative. Reducing σ repulsion is a prerequisite to make Fe—CO bonding. Again, only when both $(3d_\pi, 2\pi)^4$ and $(3d_\sigma, 4s)^2$ are included in the active space can we have a qualitatively correct picture of the Fe—CO bonding.

Figure 3 depicts the contour plots of frontier σ orbitals emerged from $(3d_\pi, 2\pi)^4(3d_\sigma, 4s)^2(3d_\delta)^2$/CAS(8, 8) calculation. Figure 4 presents the difference contour plots obtained by the electron density of CAS(8, 8) minus that of CAS(4, 4). Inclusion of π electron correlation not only enhances the π back-donation from Fe $3d_\pi$ to CO 2 π, but also increases the σ donation from CO 5σ to Fe $3d_\sigma$.

Taking the energy of the nonbounded ROHF FeCO as the reference, correlating the σ electrons leads to notable stabilization (−0.63 eV), while correlating the π electrons also brings about large

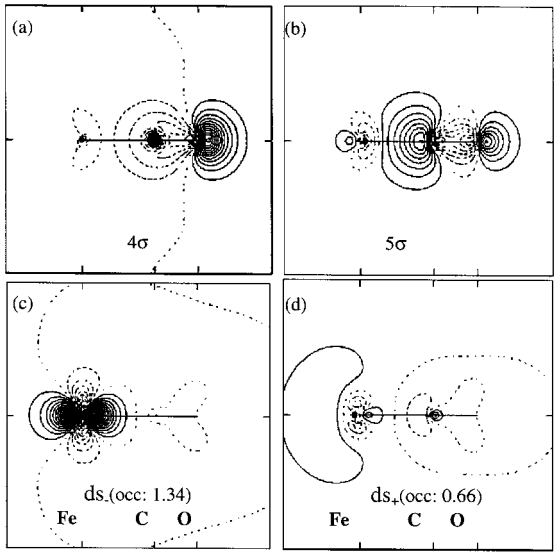

FIGURE 3. σMO plots of $^3\Sigma^-$ FeCO: (a)–(d) from $(3d_\pi, 2\pi)^4(3d_\sigma, 4s)^2(3d_\delta)^2$/CAS(8, 8).

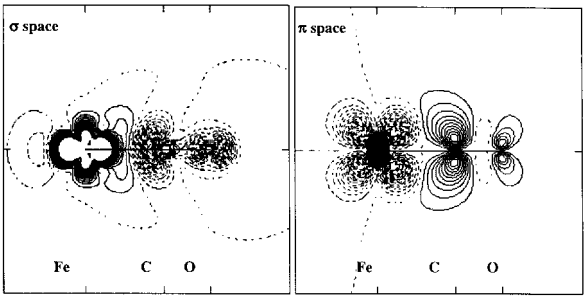

FIGURE 4. $^3\Sigma^-$ FeCO difference contour plots between $(3d_\pi, 2\pi)^4(3d_\sigma, 4s)^2(3d_\delta)^2$/CAS(8, 8) and $(3d_\sigma, 4s)^2(3d\delta)^2$/CAS(4, 4). Dashed lines indicate electron loss while solid lines indicate electron gain.

correlation energy (-1.16 eV). However, correlating both σ and π electrons results in a stabilization (-3.23 eV) which greatly exceeds the summation of the separate contributions from σ and π electrons ($-0.63 - 1.16 = -1.79$ eV). Clearly, there exists concerted σ/π interactions in FeCO. We should point out that although it seems that the π correlation energy (-1.16 eV) outweighs the σ correlation energy (-0.63 eV) we believe that in the case of FeCO it is the σ electrons that make the largest contribution to the formation of the Fe—CO bond, since it is the correlation of σ electrons that holds Fe and CO together. In fact, as the σ interactions are interdependent with π interactions (and vice versa), it is not appropriate to go into all details independently.

It is worthwhile to compare and contrast the bonding in FeCO $^3\Sigma^-$ with that in NiCO $^1\Sigma^+$. The RHF calculation on NiCO results in a Ni close to $3d^{10}$ configuration, while ROHF calculations on FeCO leads to a Fe having $3d^64s^2$ configuration. CAS calculations show that NiCO $^1\Sigma^+$ is a Ni $^1D(3d^94s^1)$-derived state with an important contribution of d^{10} at the equilibrium geometry; FeCO $^3\Sigma^-$, on the other hand, is a Fe $^3F(d^7s^1)$-derived state with little $4s \rightarrow 3d_\sigma$ excitation. This difference between NiCO and FeCO is clearly seen in the orbitals and occupation numbers. For NiCO, two correlated σ orbitals are ds_- [(g) in Fig. 1] and ds_+ [(h) in Fig. 1] hybrids. The ds_- orbital, almost doubly occupied (1.94), shifts electron density away from CO 5σ and is nonbonding; while the ds_+ orbital, antibonding to CO 5σ, is only weakly occupied (0.06). From the populations of CAS wave functions in Table II, we see that the $4s$ and $3d_\sigma$ populations for NiCO $^1\Sigma^+$ are around 0.55 and 1.68 electrons. This indicates a strong $4s \rightarrow 3d_\sigma$ excitation. Thus, for NiCO $^1\Sigma^+$, both sd_σ hybridization and $3d^94s^1/3d^{10}$ mixing mechanisms are in effect. For FeCO $^3\Sigma^-$, on the other hand, both two-correlated σ orbitals are occupied. The occupations of ds_- [(d) in Fig. 3] and ds_+ [(d) in Fig. 3] are 1.34 and 0.66 electrons. There is significant p_σ mixed in ds_+ [cf. (h) in Fig. 1 and (d) in Fig. 3]. Therefore, both sd_σ hybridization and sp_σ hybridization occur in FeCO $^3\Sigma^-$. The CI weight of the main configuration-state function in the CAS wave function of FeCO $^3\Sigma^-$ is only 0.56. From the $4s$ and $3d_\sigma$ populations of CAS wave functions in Table IV, we may conclude that there is little $4s \rightarrow 3d_\sigma$ excitation in FeCO $^3\Sigma^-$. Comparing the calculated molecular properties summarized in Tables I and III, we can see that there is a larger downshift of the CO stretching frequency in FeCO than that in NiCO, accompanied by a longer CO bond distance in FeCO. This indicates a larger π donation from metal $3d_\pi$ to CO 2π in FeCO than that in NiCO. On the other hand, the Ni—C stretching frequency is larger than the Fe—C stretching frequency and the Ni—C bond distance is shorter than the Fe—C bond distance. This in accord with the experimental findings, namely, the dissociation energies for the ground states NiCO and FeCO are 29 ± 15 kcal/mol [33] and 8.1 ± 3.5 kcal/mol [34].

All these differences in bonding between NiCO and FeCO may be traced back to the differences between atomic Fe and Ni. After weight-averaging the spin–orbit fine-structure splittings, we have Ni $^3D(3d^94s^1)$ as the ground state [13]. Ni $^1D(3d^94s^1)$ is only 0.33 eV higher and $^1S(3d^{10})$ is also not far (1.74 eV) from the ground state [13]. Therefore, there is a high possibility to mix $3d^{10}$ with $3d^94s^1$ so as to facilitate the Ni—CO bonding. For Fe, $^5D(3d^64s^2)$ is the ground state [13]. The groundsate FeCO $^3\Sigma^-$ is derived from Fe $^3F(3d^74s^1)$ [18], which is 1.49 eV above the ground state of Fe [13]. The Fe $^3F(d^8)$, being so much higher (4.07 eV) in energy [13], can hardly make any important contribution to FeCO bonding. For Ni, the lowest-lying state with $4p$ occupation is $^4D^0(3d^84s^14p^1)$, which is 3.2 eV above the ground state, while $^1P^0(3d^94p^1)$ is 4.0 eV higher in energy [13]. On the other hand, the lowest-lying state with $4p$ occupation for Fe is only 2.38 eV higher, and there exist eight terms with $4p$ occupied between Fe $^3F(3d^74s^1)$ and $^3F(3d^8)$ [13]. Therefore, sp_σ hybridization is easier for FeCO than for NiCO. Experimentally, the Ni $^2D(3d^9) \leftarrow$ Ni $^1S(3d^{10})$ ionization energy is 8.7 eV, while the Ni $^2F(3d^84s^1) \leftarrow$ Ni $^1D(3d^94s^1)$ ionization energy is 11.8 eV [13]. Based on this energetic information, one may understand why it is important to mix the $3d^{10}$ configuration into the $3d^94s^1$ configuration in NiCO in terms of enhancement of the π donation. Along this line, the π donation in FeCO is expected to be more significant because of the lower Fe $^4D(3d^64s^1) \leftarrow$ Fe $^3F(3d^74s^1)$ ionization energy (7.7 eV) [13]. On the other hand, the higher occupation of the $4s$ orbital in FeCO than that in NiCO offsets the more favorable π bonding and should be responsible for the weaker binding energy in FeCO than that in NiCO.

Conclusions

We performed a series of CASSCF calculations with different choices of active spaces. In this graduated CASSCF scheme, we examined the changes on the electronic structures and geometric structures of NiCO and FeCO, as well as the energy lowering by considering only the σ correlation or the π correlation and the σ/π correlation together. The methodology used presented a pertinent illustration of the role of correlation effects in metal–ligand bonding. Our calculations have set up a good relationship between the Blyholder model and the Bagus model, that is, the σ space is indeed mainly repulsive, in agreement with Bagus, while there does exist a synergistic σ/π interaction, in agreement with Blyholder. The main features of the interactions in M—CO can be summarized as follows:

1. The metal–CO bonding would be better described as σ-polarization to reduce σ repulsion between metal $4s$ and CO 5σ and π donation from metal $3d_\pi$ to CO 2π. The σ donation from CO 5σ to metal d_σ or $d_\sigma sp_\sigma$ hybrids does exist, but is less important.
2. There does exist a synergistic σ/π interaction between the metal and the CO group. Only when both σ/π spaces are correlated can we have a qualitatively correct picture of the M—CO bonding. Reducing the σ repulsion brings the metal and CO closer, enhancing the π donation from metal d_π to CO 2π. On the other hand, π bonding offsets the energy cost for $4s \rightarrow 3d_\sigma$ excitation as well as the sdp_σ hybridization and leads to more favorable σ interaction.
3. The relative importance of σ/π interactions depends on the nature of the metal. Since the ground state of Fe is $^5D(3d^64s^2)$, to decrease the large σ repulsion is the prerequisite to result in a net Fe—CO bonding; therefore, σ interaction is more important than is π interaction. In the case of NiCO, as Ni $^1D(3d^94s^1)$ and Ni $^1S(3d^{10})$ are not very far from the ground state of Ni $^3D(3d^94s^1)$, π donation makes the largest contribution to the stability of NiCO.

ACKNOWLEDGMENTS

This work was supported by the National Natural Science Foundation of China, the specific doctoral project foundation sponsored by the State Education Commission of China, the Fok Ying Tung Education Foundation, and the Japan Society for Promotion of Science.

References

1. Fournier, R. J Chem Phys 1993, 99, 1801.
2. Veillard, A. Chem Rev 1991, 91, 743.
3. Daoudi, A.; Suard, M.; Berthier, G. J Mol Struct (Theochem) 1990, 210, 139.
4. Blyholder, G. J Chem Phys 1962, 36, 2036; 1966, 44, 3134.
5. Bagus, P. S.; Nelin, C. J.; Bauschlicher, C. W. Phys Rev B 1983, 28, 5423.
6. Bauschlicher, C. W.; Bagus, P. S. J Chem Phys 1984, 81, 5889.
7. Bagus, P. S.; Hermann, K.; Bauschelicher, C. W. J Chem Phys 1984, 80, 4378.
8. Bauschlicher, C. W.; Bagus, P. S.; Nelin, C. J.; Roos, B. O. J Chem Phys 1986, 85, 354.
9. Blyholder, G.; Lawless, M. J Am Chem Soc 1992, 114, 5828.
10. General discussion in Faraday Symposium 21, J Chem Soc Faraday Trans 1987, 83, 1963.
11. Rives, A. B.; Fenske, R. F. J Chem Phys 1981, 75, 1293.
12. Kao, C. M.; Messmer, R. P. Phys Rev B 1985, 31, 4835.
13. Moore, C. E. In Atomic Energy Levels, Natl. Bur. Stand. (U.S.) Spec. Pub. No. 467; U.S. General Printing Office: Washington DC, 1952; Vol. II.
14. Madhavan, P. V.; Whitten, J. L. Chem Phys Lett 1986, 127, 354.
15. Blomberg, M. R. A.; Brandemark, U. B.; Siegbahn, P. E. M.; Mathisen, K. B.; Karlström, G. J Phys Chem 1985, 89, 2171.
16. Roos, B. O.; Taylor, P. R.; Siegbahn, P. E. M. Chem Phys 1980, 48, 157.
17. Siegbahn, P. E. M.; Almlöf, J.; Heiberg, A.; Roos, B. O. J Chem Phys 1981, 74, 2381.
18. Villalta, P. W.; Leopold, D. G. J Chem Phys 1993, 98, 7730.
19. Berthier, G.; Daoudi, A.; Suard, M. J Mol Struct (Theochem) 1988, 179, 407.
20. Castro, M.; Salahub, D. R.; Fournier, R. J Chem Phys 1994, 100, 8233.
21. Persson, B. J.; Roos, B. O.; Pierloot, K. J Chem Phys 1994, 101, 6810.
22. Barnes, L. A.; Rosi, M.; Bauschlicher, C. W. J Chem Phys 1991, 94, 2031.
23. Blomberg, M.; Brandemark, U.; Johansson, J.; Siegbahn, P.; Wennerberg, J. J Chem Phys 1988, 88, 4324.
24. Wachters, A. J. H. J Chem Phys 1970, 52, 1033.
25. Hay, P. J. J Chem Phys 1977, 66, 4377.
26. van Duinjveldt, F. B. IBM Research Report No. RJ945, 1971.

27. Bauschlicher, C. W.; Pettesson, L. G. M.; Siegbahn, P. E. M. J Chem Phys 1987, 87, 2129.
28. Frisch, M. J.; Trucks, G. W.; Schlegel, H. B.; Gill, P. M. W.; Johnson, B. G.; Robb, M. A.; Cheeseman, J. R.; Keith, T. A.; Petersson, G. A.; Montgomery, J. A.; Raghavachari, K. Al-Laham, M. A.; Zakrzewski, V. G.; Ortiz, J. V.; Foresman, J. B.; Cioslowski, J.; Stefanov, B. B.; Nanayakkara, A.; Challacombe, M.; Peng, C. Y.; Ayala, P. Y.; Chen, W.; Wong, M. W.; Andres, J. L.; Replogle, E. S.; Gomperts, R.; Martin, R. L.; Fox, D. J.; Binkley, J. S.; Defrees, D. J.; Baker, J.; Stewart, J. P.; Head-Gordon, M.; Gonzalez, C.; Pople, J. A. Gaussian 94 (Revision D.2); Gaussian: Pittsburg, PA, 1995.
29. Huber, K. P.; Herzberg, G. Molecular Spectra and Molecular Structure; Constants of Diatomic Molecules, Vol. IV; Van Nostrand: Princeton, 1979.
30. Sodupe, M.; Bauschlicher, C. W.; Lee, T. J. Chem Phys Lett 1992, 189, 266.
31. DeKock, R. L. Inorg Chem 1971, 10, 1205.
32. Blomberg, M. R. A.; Brandemark. U. B.; Siegbahn, P. E. M.; Wennerberg, J.; Bauschlicher, C. W. J Am Chem Soc 1988, 110, 6650.
33. Stevens, A. E.; Feigerle, C. S.; Lineberger, W. C. J Am Chem Soc 1982, 104, 5026.
34. Sunderlin, L. S.; Wang, D.; Squires, R. B. J Am Chem Soc 1992, 114, 2788.